AGU PUBLICATIONS

JGR

Journal of Geophysical Research: Space Physics

RESEARCH ARTICLE
10.1002/2016JA022475

Key Points:
- Prompt penetration electric field driven by solar wind density
- Equatorial electric field disturbance under northward IMF B_z
- Signatures in global magnetic data and geosynchronous count rate

Correspondence to:
D. Rout,
diptir@prl.res.in

Citation:
Rout, D., D. Chakrabarty, R. Sekar, G. D. Reeves, J. M. Ruohoniemi, T. K. Pant, B. Veenadhari, and K. Shiokawa (2016), An evidence for prompt electric field disturbance driven by changes in the solar wind density under northward IMF B_z condition, *J. Geophys. Res. Space Physics*, *121*, doi:10.1002/2016JA022475.

Received 2 FEB 2016
Accepted 28 APR 2016
Accepted article online 2 MAY 2016

An evidence for prompt electric field disturbance driven by changes in the solar wind density under northward IMF B_z condition

Diptiranjan Rout[1], D. Chakrabarty[1], R. Sekar[1], G. D. Reeves[2], J. M. Ruohoniemi[3], Tarun K. Pant[4], B. Veenadhari[5], and K. Shiokawa[6]

[1]Physical Research Laboratory, Ahmedabad, India, [2]Los Alamos National Laboratory, Los Alamos, New Mexico, USA, [3]Bradley Department of Electrical and Computer Engineering, Virginia Polytechnic Institute and State University, Blacksburg, Virginia, USA, [4]Space Physics Laboratory, VSSC, Thiruvananthapuram, India, [5]Indian Institute of Geomagnetism, Navi Mumbai, India, [6]ISEE, Nagoya University, Nagoya, Japan

Abstract Before the onset of a geomagnetic storm on 22 January 2012 ($Ap = 24$), an enhancement in solar wind number density from 10/cm^3 to 22/cm^3 during 0440–0510 UT under northward interplanetary magnetic field (IMF B_z) condition is shown to have enhanced the high-latitude ionospheric convection and also caused variations in the geomagnetic field globally. Conspicuous changes in ΔX are observed not only at longitudinally separated low-latitude stations over Indian (prenoon), South American (midnight), Japanese (afternoon), Pacific (afternoon) and African (morning) sectors but also at latitudinally separated stations located over high and middle latitudes. The latitudinal variation of the amplitude of the ΔX during 0440–0510 UT is shown to be consistent with the characteristics of prompt penetration electric field disturbances. Most importantly, the density pulse event caused enhancements in the equatorial electrojet strength and the peak height of the *F* layer (h_mF_2) over the Indian dip equatorial sector. Further, the concomitant enhancements in electrojet current and *F* layer movement over the dip equator observed during this space weather event suggest a common driver of prompt electric field disturbance at this time. Such simultaneous variations are found to be absent during magnetically quiet days. In absence of significant change in solar wind velocity and magnetospheric substorm activity, these observations point toward perceptible prompt electric field disturbance over the dip equator driven by the overcompression of the magnetosphere by solar wind density enhancement.

1. Introduction

During space weather events, several types of prompt electric field disturbances affect equatorial ionosphere almost instantaneously. These include electric fields due to the undershielding [*Chakrabarty et al.*, 2005, 2006] and overshielding effects [*Fejer et al.*, 2007; *Sekar and Chakrabarty*, 2008] associated with IMF B_z (or IEF_y), penetration electric field associated with IMF B_y [*Kelley and Makela*, 2002], induction electric field due to dipolarization of geomagnetic field at the substorm onset [*Kikuchi et al.*, 2003; *Chakrabarty et al.*, 2015], and induced electric field due to the compression of equatorial magnetic flux owing to the increase in the solar wind dynamic pressure. The transient electric field disturbances during storm sudden commencements (SSCs) [*Sastri et al.*, 1993] or sudden impulses (SIs) [*Akasofu and Chao*, 1980] or main impulse (MI) [*Sastri et al.*, 1993] fall in the last category. These events are mostly associated with the enhancement in the dynamic (ram) pressure during the passage of interplanetary shocks. Interplanetary shocks are primarily governed by changes in the solar wind velocity, and these events have been reported earlier. However, it remains to be observed whether changes in the solar wind density affect equatorial ionospheric electric fields. Till date, to the best of these authors' knowledge, evidence for the changes in the equatorial ionospheric electric field due to changes dominated by the solar wind density alone is not available. One of the reasons for this is the simultaneous changes in the solar wind velocity and density during most of the ram pressure enhancement events. Further, during southward IMF B_z conditions, other kinds of prompt electric field disturbances (mentioned earlier) can be present to obfuscate the effects due to change in the solar wind density alone.

In recent times, a few efforts have been made to capture the changes in the equatorial ionosphere corresponding to changes in the solar wind ram pressure. For example, *Zong et al.* [2010] showed reduction in equatorial

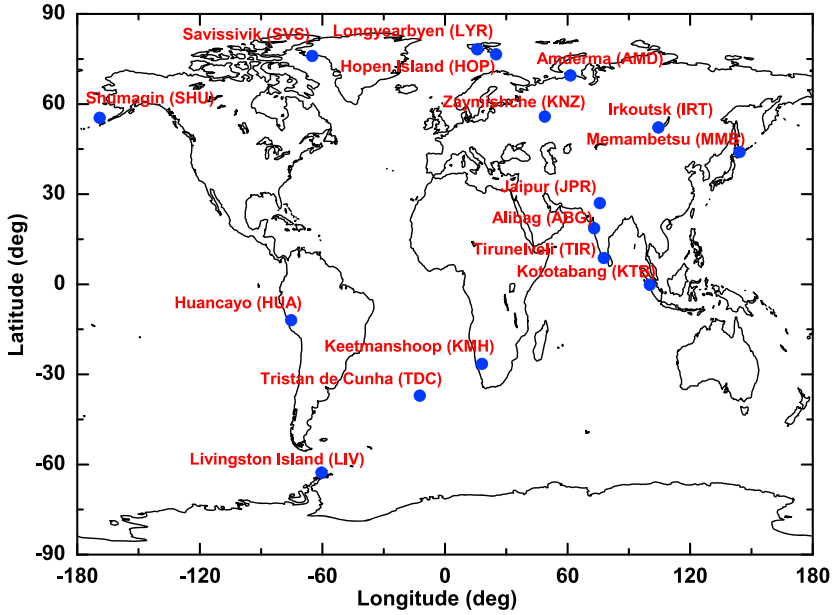

Figure 1. A global map with the magnetometer stations marked on it. Magnetic data from these stations are used in the present study.

total electron content corresponding to an interplanetary shock. This shock is associated with changes in the solar wind ram pressure due to simultaneous changes in velocity and density under the northward IMF B_z condition. On the other hand, *Yuan and Deng* [2007] indicated the role of continuous solar wind pressure variations on the long-lasting penetration of the interplanetary electric field in the equatorial ionosphere during southward IMF B_z condition. In addition, *Huang et al.* [2008] showed that ion velocities over Jicamarca increased following enhancements in the ram pressure regardless of the polarity of IMF B_z. Although such events can throw light on the effects of solar wind ram pressure on the equatorial ionosphere, the role of density is not explicitly evident based on these observations. Recently, *Wei et al.* [2012] showed significant effect of solar wind density in controlling the prompt electric field disturbance at the equatorial ionosphere during a polar cap saturation event. In their study, the density effects are studied primarily during the main phase of a storm when IMF B_z is southward. In fact, a few global MHD simulations [*Slinker et al.*, 1999; *Lopez et al.*, 2004] have indicated the role of solar wind density on the magnetosphere and ionosphere. However, observational evidence for the presence of prompt electric field disturbance in the equatorial ionosphere driven solely by changes in the solar wind density under northward IMF B_z conditions is still unavailable. The present investigation, based on a case study, provides evidence that the equatorial ionospheric electric field changes nearly simultaneously corresponding to a change in the solar wind density under northward IMF B_z condition.

2. Data Set

The solar wind parameters (like solar wind velocity, density, and magnetic field) are taken from the NASA Goddard Space Flight Center (GSFC) Coordinated Data Analysis Web (CDAWeb) (http://cdaweb.gsfc.nasa.gov/) wherein solar wind parameters are corrected for propagation lag till the bow shock nose. The temporal resolution of solar wind parameters is 1 min. The indices like *SYM-H* (symmetric component of ring current) and *AL* (westward auroral electrojet) are taken from CDAweb with 1 min temporal resolution. The northward component (X) of the geomagnetic field measured at a few longitudinally separated low-latitude stations in the Indian, Japanese, African, South American, and Pacific sectors is used in the present study. In addition, measurements of X from a few high, middle and low latitude stations in the Northern and Southern Hemispheres are also investigated to capture the latitudinal changes. The ΔX variation for a given station is obtained after subtracting the nighttime base value level. The temporal resolution of the ΔX data is 1 min. Figure 1 shows the global map on which the magnetometer stations are marked from where the data sets are used in the present investigation. The ΔX data from these stations are used to construct Figures 3 and 4 which will be presented in section 3. It is to be mentioned here that with the exception of three Indian

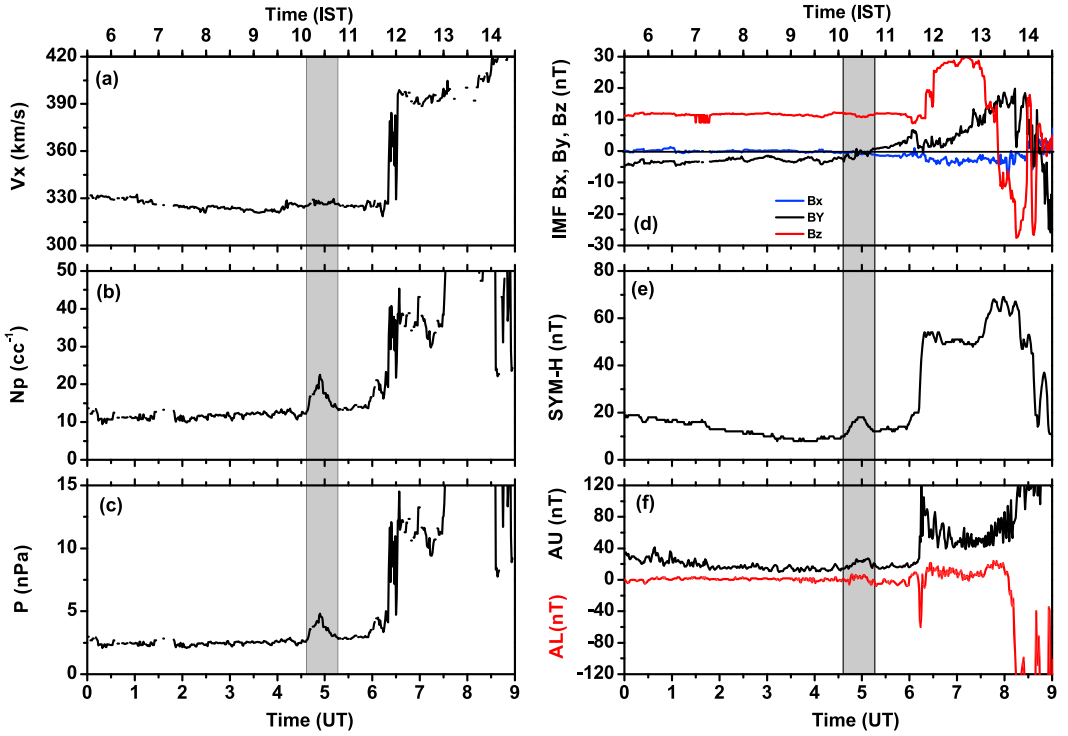

Figure 2. Variations in (a) solar wind velocity; (b) solar wind density; (c) solar wind ram pressure; (d) IMF B_x (blue), B_y (black), and B_z (red); (e) *SYM-H*; and (f) *AL* (red) and *AU* (black), respectively, during 0000–0900 UT on 22 January 2012. Corresponding time in IST is also shown at the top. The gray shaded rectangular box marks the interval when increase in solar wind density is observed under steady solar wind velocity and northward IMF B_z conditions.

stations (TIR, ABG, and JPR) and one Japanese station (KTB), all the other representative magnetic data are taken from SuperMAG network (http://supermag.jhuapl.edu).

In absence of direct ionospheric electric field measurements over the Indian dip equatorial sector, magnetometer and ionosonde measurements are used to infer the electric field perturbations during the event under consideration. It is known that ΔH_{TIR}-ΔH_{ABG} represents the difference in the variation in the horizontal component of geomagnetic field over an equatorial (TIR) and an off-equatorial station (ABG) in the Indian sector. Therefore, this difference cancels out the magnetospheric contribution (not expected to change significantly between TIR and ABG) and can be taken to represent ionospheric contributions only. This methodology proposed by *Rastogi and Patil* [1986] is shown to represent the *E* region electric field variations that are responsible for the changes in electrojet current during daytime over the Indian dip equatorial region. As the precision of the magnetic measurements are very high (~0.1 nT), small variations in the EEJ strength can be captured by this technique.

In order to verify the presence of prompt electric field disturbances over the dip equatorial ionosphere using measurements from another independent technique (other than magnetometer), digisonde measurement over Thumba (geographic latitude: 8.5°N; geographic longitude: 77°E and dip: 0.5°N) is used. It is known that ionospheric layer heights (e.g., $h'F$, h_mF_2) respond to the electric field variations over the dip equator. However, the virtual base height of the *F* layer ($h'F$) cannot be used to infer the electric field disturbances as it is also affected by production (during daytime) and loss (during both day and nighttime) processes. On the other hand, the peak height of the F_2 layer (h_mF_2) is minimally affected by loss processes as it is above 300 km [*Bittencourt and Abdu*, 1981] on most occasions. Further, in the absence of solar flare events, fast changes in h_mF_2 during daytime is unlikely to be caused by production processes. Therefore, variation in h_mF_2 is used in the present investigation to additionally confirm the electrodynamical perturbations associated with the space weather event under consideration. The h_mF_2 values are scaled using the ARTIST software [*Reinisch and Huang*, 2001]. The typical uncertainty in the determination of h_mF_2 during daytime is ~5 km.

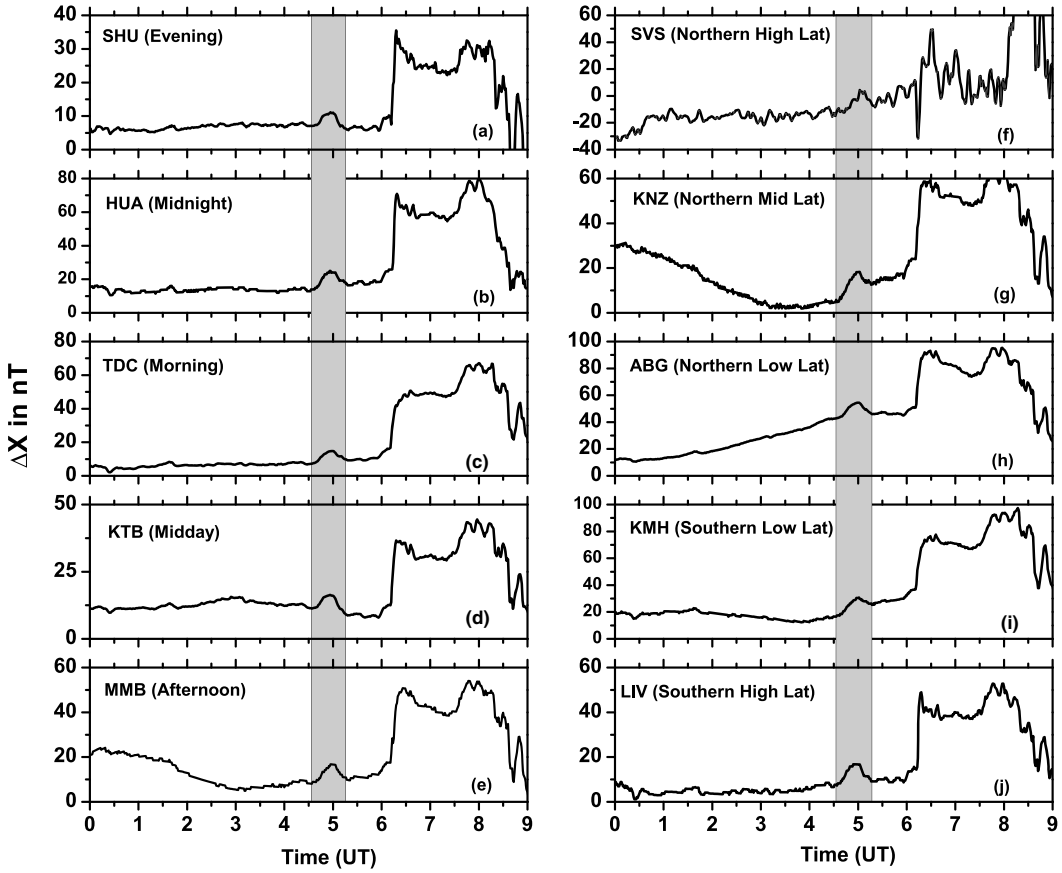

Figure 3. The ΔX variations for a few (a–e) longitudinally and (f–j) latitudinally separated stations during 0000–0900 UT. The longitudinally separated stations (SHU, HUA, TDC, KTB, and MMB) represent different local times that are mentioned in the figure. The latitudinally separated stations (SVS, KNZ, ABG, KMH, and LIV) include Northern and Southern Hemispheric stations. It can be noted that the ΔX variations during 0440–0510 UT (marked by vertical shaded region) show distinct enhancements irrespective of longitude and latitude.

3. Results

Figures 2a–2c reveals the variation in the solar wind velocity (V_x, in km/s), proton density (N_p, in /cm^3), and dynamic pressure (P, in nPa) during 0000–0900 UT (universal time) on 22 January 2012. Corresponding Indian Standard Time (IST = UT + 5.5 h) is also shown on top of Figures 2 and 5 to facilitate interpretation of Figure 5 which is used to infer the ionospheric prompt electric field perturbations over the Indian dip equatorial sector. Figure 2d shows the variations in IMF B_x (in blue), IMF B_y (in black), and IMF B_z (in red) in nanotesla, respectively, during the same interval. It is clearly seen that solar wind parameters like V_x and IMF B_z do not show significant changes during 0440–0510 UT (marked by vertical shaded box). IMF B_y starts changing its polarity during this interval and remains very close to zero at ~0450 UT when a peak in the solar wind density is observed. This enhancement (and not the larger enhancement during the onset of SSC at 0612 UT) in the solar wind density is of interest here as this occurs in the absence of any significant change in the solar wind velocity. IMF B_x also remains almost constant during this interval. Solar wind density changes from 10/cm^3 to 22/cm^3 during 0440–0510 and maximizes at ~0450 UT. In contrast, velocity (V_x) during this interval changes by only 2 km/s. The solar wind ram pressure changes from 2.5 nPa to 5 nPa during 0440–0510 UT. Small but detectable changes are observed in *AU* (black) and *AL* (red) (see Figure 2f) during this interval. The change in *SYM-H* (Figure 2e) is ~10 nT which is significant. It must be noted that IMF B_z is northward during this time. In addition to the above event, both V_x and N_p register sharp enhancements at 0618 UT under northward IMF B_z condition. In fact, a storm sudden commencement (SSC) occurs at 0612 UT due to the arrival of the associated interplanetary shock at this time. The SSC is followed by an initial phase that continues for ~2 h. As the earlier SSC-related prompt electric field penetration effects [*Sastri et al.*, 1993] did not explicitly attempt to delineate

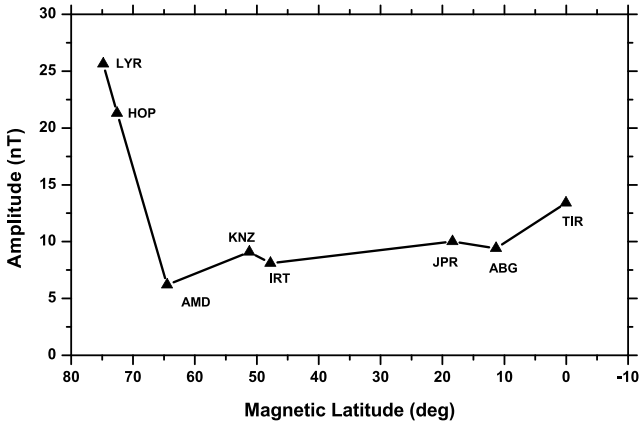

Figure 4. Latitudinal variation in the amplitude (in nT) of ΔX during the 0440–0510 UT at the dayside stations spanning from polar region to dip equatorial regions. Dip equatorial enhancement in ΔX can be seen. It can also be noticed that amplitude over the dip equator is comparable to that over the subauroral region and less than that over the polar region.

the impact of solar wind density alone, the present investigation fills this gap by identifying an event where solar wind density changes but not the solar wind velocity.

In order to find out the effects of the solar wind density pulse during 0440–0510 UT on the global magnetic field, Figure 3 is presented. Figures 3a–3e and Figures 3f–3j show ΔX variations at a few longitudinally and latitudinally separated stations, respectively, during 0000–0900 UT. The longitudinally separated stations represent different local time sectors (mentioned in the figure), while the latitudinally separated stations represent high, middle, and low latitudes (not along the same meridian) from Northern and Southern Hemispheres. It can be noticed that ΔX variations during 0440–0510 UT (marked by vertical shaded region) register distinct enhancements at all stations irrespective of longitude or latitude corresponding to the density-related pressure enhancement. Therefore, Figure 3 elicits the global nature of the ΔX enhancement during 0440–0510 UT.

In order to confirm whether the variation in ΔX with latitude follow the characteristic pattern associated with the prompt penetration electric field and not the pattern associated with the magnetopause

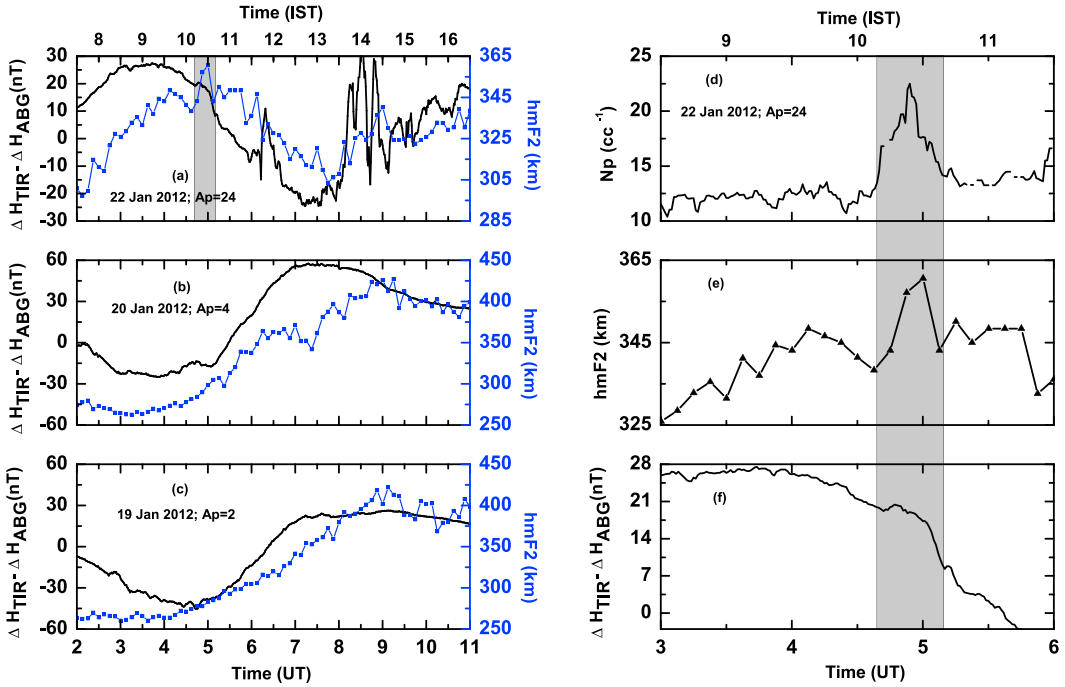

Figure 5. (a–c) The variations in ΔH_{TIR}-ΔH_{ABG} (black) and h_mF_2 (blue) during 0200–1100 UT on (Figure 5a) 22 January, vis-á-vis (Figure 5b) 20 January, and (Figure 5c) 19 January 2012 that are magnetically quiet days. The gray shaded region in Figure 5a shows the interval when simultaneous fluctuations are observed in ΔH_{TIR}-ΔH_{ABG} and h_mF_2. (d–f) The zoomed-in variations in (Figure 5e) ΔH_{TIR}-ΔH_{ABG} and (Figure 5f) h_mF_2 vis-á-vis N_p during 0300–0600 UT on 22 January 2012 with the gray shaded region overlaid. The shaded region clearly shows that the enhancements in ΔH_{TIR}-ΔH_{ABG} and h_mF_2 are concomitant with the increase in N_p.

(Chapman-Ferraro) current, Figure 4 is presented. This figure shows the latitudinal variation in the amplitude (in nT) of ΔX during 0440–0510 UT by considering a few dayside stations are considered. The ΔX amplitude maximizes over the auroral region, falls off over middle and low latitudes, and enhances again over the dip equator. It is also important to note that the ΔX amplitude over the dip equator is comparable to that over the subauroral region and less than that over the polar region.

Figure 5 explores the prompt electric field perturbations, if any, over the equatorial ionosphere during 0440–0510 UT when enhancement in solar wind density (N_p) is observed in absence of any significant change in the solar wind velocity, and IMF components. Figures 5a–5c depict comparisons of the ΔH_{TIR}-ΔH_{ABG} and h_mF_2 variations during 0200–1100 UT on the event day (22 January 2012) vis-á-vis on 20 and 19 January 2012 which are magnetically quiet days ($Ap = 4$ and 2, respectively). It is noted that the slow temporal variations in ΔH_{TIR}-ΔH_{ABG} and h_mF_2 grossly agree with each other barring morning hours. The gray shaded region marked in Figure 5a shows the interval of 0440–0510 UT when the fast fluctuations in ΔH_{TIR}-ΔH_{ABG} and h_mF_2 go hand in hand. Interestingly, although fast fluctuations are present in h_mF_2 and ΔH_{TIR}-ΔH_{ABG} on quite days, simultaneous fluctuations in both the parameters (similar to the shaded region on 22 January) are absent on the two quiet days. In order to evaluate the association of the equatorial E and F region parameters (ΔH_{TIR}-ΔH_{ABG} and h_mF_2, respectively) with the variation in the solar wind density (N_p), the shaded region in Figure 5a is blown up and presented along with solar wind density (N_p) in Figures 5d–5f. Figures 5d–5f clearly elicit that the enhancements in h_mF_2 and ΔH_{TIR}-ΔH_{ABG} are concomitant with the enhancement in N_p. The implication of this observation will be addressed in the ensuing section.

4. Discussion

Solar wind dynamic (ram) pressure is expressed as follows.

$$P_{\mathrm{dyn}} = \rho v^2 \tag{1}$$

In the above expression, ρ and v are solar wind density (strictly, mass density) and velocity, respectively. Differential of (1) yields the following expression.

$$\Delta P_{\mathrm{dyn}} = v^2 \Delta\rho + 2v\rho\Delta v \tag{2}$$

Based on (2), three different conditions can be envisaged through which solar wind dynamic pressure can be changed. These conditions are as follows.

Condition 1: $v\Delta\rho \approx 2\rho\Delta v$
Condition 2: $v\Delta\rho < 2\rho\Delta v$
Condition 3: $v\Delta\rho > 2\rho\Delta v$

During most of the SSC, SI, or MI events, conditions 1 or 2 get satisfied and these cases, as mentioned in section 1, have been studied in the past. However, evidence for the changes in the ionospheric electric field satisfying condition 3 is not available in the literature particularly when IMF B_z is northward. In the present case, the solar wind velocity is ~330 km/s and density is ~10/cm^3 before the arrival of the density pulse centered at 0450 UT. During the density pulse event, the maximum change in solar wind density is 12/cm^3 and the change in the solar wind velocity (Δv) is not significant (~2 km/s). Slow and nearly constant (in time) solar wind speed coupled with changes in the solar wind density makes the term $v\Delta\rho$ larger than $2\rho\Delta v$. Therefore, temporal changes in ram pressure during this time are primarily driven by the temporal changes in the solar wind density.

It must also be noted at this point that IMF B_z and B_y remain nearly steady when changes in $\Delta\rho$ occur during 0440–0510 UT. In order to rule out influence of any substorm-induced transient electric field at this time, the geosynchronous electron and proton counts per second measured by the Los Alamos National Laboratory (LANL) satellites are shown in Figure 6. Although data from all the LANL satellites are investigated, observations from a single nightside satellite (1991-080) are presented here for brevity. Electron counts per second (Figure 6a) in four energy channels (E1: 48.15–69.85 keV; E2: 68.5–102.5 keV; E3: 99.95–149.45 keV; E4: 145.6–220.6 keV) and proton counts per second (Figure 6b) in three energy channels (P2: 75–113 keV; P3: 113–170 keV; P4: 170–250 keV) are shown. The signature of "dispersionless" injection, which is a telltale signature of substorm onset, is absent during 0440–0510 UT. Instead, one can see the characteristic undulations in the flux patterns in response to the enhancement in the ram pressure enhancement similar to what was shown earlier by *Lee et al.* [2005].

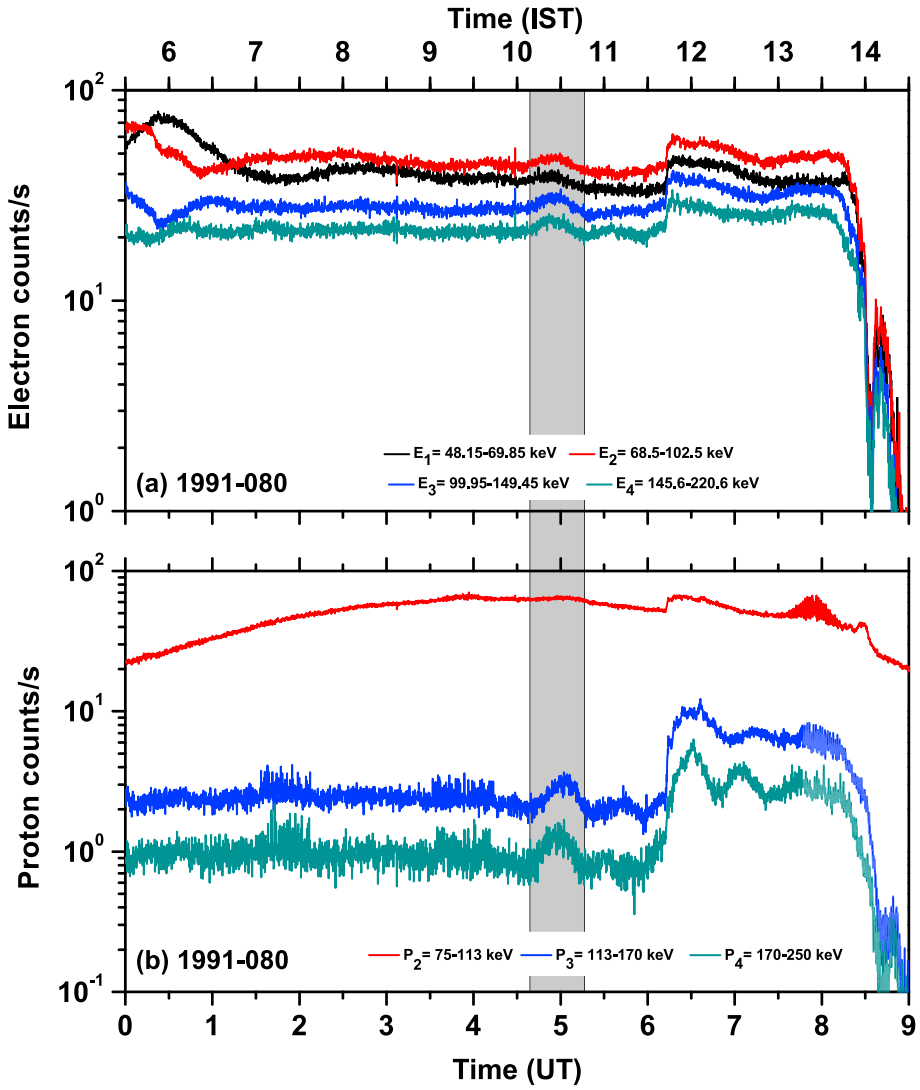

Figure 6. The changes in energetic (a) electron and (b) proton counts per second observed by LANL (1991-080) satellite during 0000–0900 UT on 22 January 2012. The gray shaded rectangular box highlights the interval (0440–0510 UT) of solar wind density enhancement.

Before addressing the electric field perturbations over the Indian dip equatorial sector, it is important to verify that the ionospheric plasma convection got enhanced over high latitudes during this density pulse event. Figures 7–9 in which three high-latitude ionospheric convection maps generated by the Super Dual Auroral Radar Network (SuperDARN) HF radar network are shown corresponding to the representative intervals of 0440–0442 UT, 0450–0452 UT, and 0510–0512 UT, respectively. An anticlockwise ionospheric flow vortex can be seen to get maximized (see red arrows) during 0450–0452 UT (Figure 8). This provides a strong evidence for the generation of region 1 field-aligned currents (R1-FACs) [e.g., *Sofko et al.*, 1995] and presence of convection electric field over high latitudes in the dawn-to-dusk direction during the density pulse event. This electric field can penetrate to lower latitudes nearly simultaneously. Further, the concomitant magnetic variations in the Indian (prenoon), South American (midnight), Japanese (afternoon), Pacific (afternoon), and African (morning) sectors as well as at the high- and middle-latitude stations during 0440–0510 UT suggest that the global ionospheric current system responded to the changes in the solar wind density during this time. Moreover, the enhancement (~10 nT) in *SYM-H* corresponding to this solar wind density enhancement is also consistent with the work of *Araki et al.* [1993] who showed that the dynamic pressure dependence of

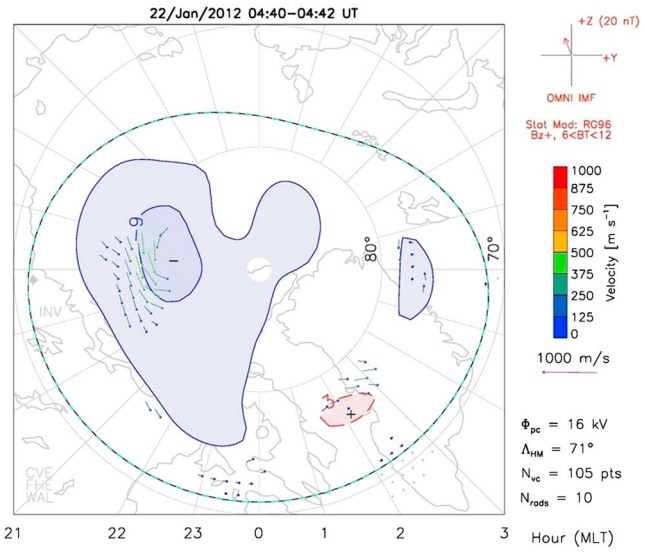

Figure 7. The high-latitude ionospheric convection maps generated by the SuperDARN HF radar network during 0440–0442 UT. High-latitude ionospheric convection is weak at this time.

the *Dst* index is essentially controlled by solar wind density irrespective of northward or southward IMF B_z condition. However, *Araki et al.* [1993] did not investigate the presence of prompt electric field disturbances over the dip equatorial ionosphere during the intervals when the solar wind density is changing. As there was no solar flare at this time 0440–0510 UT, the change in the ionospheric current system over low-equatorial latitudes is not associated with changes in ionization and most likely associated with the changes in *E* region electric field. Further, as IMF B_y does not change its polarity sharply during 0440–0510 UT when IMF B_z is northward, it is unlikely that the mechanism offered by *Kelley and Makela* [2002] is operational here.

It is clear from Figure 4 that the amplitude of ΔX during 0440–0510 UT at the dayside stations maximizes over the auroral region, falls off over middle and low latitudes, and enhances again over the dip equator. As the ΔX amplitude over the polar region is more than those over the subauroral and dip equatorial regions, the latitudinal variation depicted in Figure 4 points toward the presence of prompt penetration electric field during this interval [*Araki*, 1977; *Kobea et al.*, 2000; *Kikuchi et al.*, 2000]. It is to be noted here that in the case of significant enhancement of magnetopause (Chapman-Ferraro) current, one would have expected ΔX amplitude over the dip equator exceeding that over the polar region [*Namikawa et al.*, 1964]. On the other hand, in the prompt penetration scenario, the ionospheric Hall current driven by the high-latitude electric field closes through the Pedersen current over the dip equator and hence can generate polarization electric field when its flow is obstructed at the terminator. The ionospheric Pedersen current over the dip equator also gets amplified [*Sastri et al.*, 2003] due to Cowling conductivity. Therefore, Figure 4 is consistent with the latitudinal characteristics of prompt penetration electric field, and the generation of this electric field in the present case is associated with the enhancement in solar wind density.

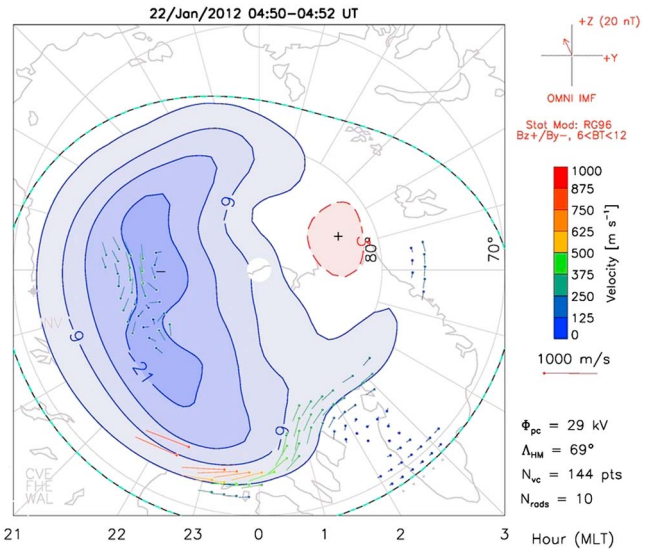

Figure 8. Same as Figure 7 but for the interval 0510–0512 UT. An anticlockwise and enhanced (see red arrows) ionospheric flow vortex can be seen at this time.

Figure 5 brings out the dip equatorial ionospheric signatures of the prompt penetration electric field associated with the solar wind density pulse event. Unambiguous enhancement in ΔH_{TIR}-ΔH_{ABG} (as shown in Figure 5f) when the background variation is decreasing suggests the enhancement in the eastward electric field perturbation in the *E* region during 0440–0510 UT (the shaded interval). Further, the significant rise (by about 23 km) of h_mF_2 over Thumba (Figure 5e) during the same interval suggests the presence of eastward electric field perturbation in the *F* region. The efficacy of h_mF_2 in promptly capturing the electric field

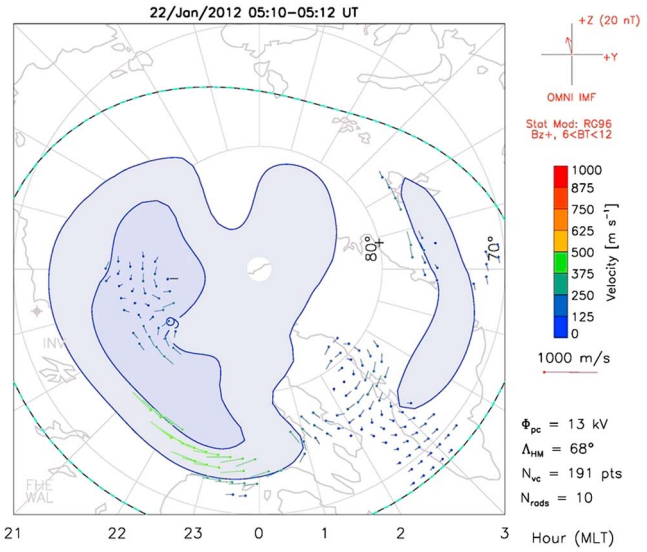

Figure 9. Same as Figure 7 but for the interval 0510–0512 UT. The anticlockwise ionospheric flow vortex is seen to be weakened substantially at this time.

disturbance over the dip equatorial region during storm time is shown by several researchers [*Szuszczewicz et al.*, 1998; *Yue et al.*, 2008]. In the present case, considering a 5 km uncertainty in the determination of h_mF_2, the increase in the *F* layer vertical drift during 0438–0506 UT turns out to be ~16.81 ± 5.2 m s^{-1}. Therefore, simultaneous increases in both h_mF_2 and ΔH_{TIR}-ΔH_{ABG} during 0440–0510 UT on 22 January 2012 point toward the prompt electric field disturbance [e.g., *Tsurutani et al.*, 2004; *Sekar et al.*, 2012; *Abdu et al.*, 2013]. Figures 5b and 5c suggest that this does not happen all the time. Although one can observe small temporal scale fluctuations in h_mF_2 and ΔH_{TIR}-ΔH_{ABG} on 20 January as well as on 19 January 2012, those are not simultaneous fluctuations. This indicates toward the electric field effects of local origin. Therefore, small temporal scale fluctuations that occurred simultaneously in the dip equatorial *E* and *F* regions during 0440–0510 UT when solar wind density got enhanced strongly point toward the imposition of prompt electric field disturbance on the equatorial ionosphere. Measurements by a number of independent techniques spread over the globe provide credence to this proposition. The possible mechanisms through which the equatorial ionosphere can get affected due to the enhancement of solar wind density are addressed in the ensuing paragraph.

The electric field disturbances for about 30–40 min over the dip equatorial ionosphere during enhancements in the solar wind ram pressure was shown by *Huang et al.* [2008] using Jicamarca drift data. The distinctive point where this investigation is different from the work of *Huang et al.* [2008] is primarily the isolation of the role of solar wind density in causing the prompt electric field disturbance. As discussed in *Huang et al.* [2008], there are two possible mechanisms through which enhancement in solar wind ram pressure can cause prompt electric field disturbance over the equatorial ionosphere. The first mechanism is through the overcompression of the magnetosphere when the solar wind ram pressure enhances. In fact, the compression or decompression of magnetospheric plasma can reach ionosphere by the Alfven and magnetosonic waves [e.g., *Tamao*, 1964; *Lysak and Lee*, 1992; *Lyatsky et al.*, 2010]. *Keller et al.* [2002] suggest that as the solar wind density pulse propagates along the flank of the magnetopause, a two-step response in field-aligned current (FAC) is expected. In the first step, FACs increase near the polar cap, and in the second step, the FACs increase near the low latitude. The increase in FAC is also found to be in the same direction as that of region 1 currents. This implies that the azimuthal electric field, which is generated inside the magnetosphere due to the earthward motion of the compressed magnetospheric plasma, can penetrate into the low-latitude ionosphere [*Shi et al.*, 2009; *Lyatsky et al.*, 2010]. Therefore, this situation is different from the conventional prompt penetration scenario in terms of place of origin of the electric field. In the conventional prompt penetration scenario, the electric field exists in the solar wind with respect to Earth, whereas in this case the electric field is generated inside the magnetosphere. This situation is probably similar to the overcompression mechanism discussed by *Huang et al.* [2008]. The distinctive feature associated with this mechanism is the enhancement of the geomagnetic field at all local times. This is what is observed in the present case. The other mechanism is similar to what was proposed by *Araki* [1994] to explain the main impulse in the low-latitude geomagnetic field in response to solar wind pressure enhancement. The model of *Araki* [1994] suggests that the low-latitude geomagetic response to the enhancement in the solar wind ram pressure comprises a preliminary impulse (~1 min), a main impulse (~10 min), and a step-like increase that continues for some time. While the preliminary impulse and the main impulse are believed to be due to R1-FAC and ionospheric currents, the step-like increase is caused by the magnetopause current. The characteristic feature in this scenario is the local time differences in the geomagnetic field response. In fact, according to the work of *Araki* [1994] and *Araki et al.* [2006], the effect of main

impulse is expected to be highest in the nightside and nominal in the dayside. It can be noted that the present set of observations are not consistent with both the step-like and local time variations in the geomagnetic field features expected from the Araki mechanism. Therefore, the prompt electric field disturbance reported in the present case arose most likely due to the associated effects of overcompression of the magnetosphere due to the density-related changes in the solar wind ram pressure.

Last but not the least, it is important to note that the prompt electric field disturbances presented in this investigation occurs essentially through the increase in the ram pressure. However, based on a case study, it is rather difficult to comment on the differences in the ionospheric effects corresponding to change in solar wind density or velocity. More investigations are needed to address this issue. Further, the mechanism through which magnetosphere is coupled with low-latitude ionosphere during the density pulse events is not comprehensively understood. In addition, as the ionospheric electric fields are curl free, it is expected that the electric field disturbances will have opposite polarity at conjugate longitudes. However, it is not clear how the ionospheric electric field will adjust globally if magnetosphere is compressed asymmetrically by solar wind ram pressure. Global measurements are needed to address this aspect comprehensively.

5. Summary

This case study, based on a unique set of measurements, reveals that a transient change in solar wind density from 10/cm^3 to 22/cm^3 during 0440–0510 UT under northward IMF B_z condition has not only enhanced the high-latitude convection but also enhanced the global magnetic field as well as equatorial *E* and *F* region electric field simultaneously. The enhanced high-latitude ionospheric convection, latitudinal characteristics of the increase in the geomagnetic field strength, enhancement of the geomagnetic field at all local times and the concomitant changes in the equatorial *E* and *F* region parameters elicit the role of solar wind density in generating transient electric field disturbances over the dip equatorial ionosphere through the associated effects of overcompression of the magnetosphere.

Acknowledgments

Magnetic data from the three Indian stations (TIR, ABG, and JPR) are provided by Indian Institute of Geomagnetism, India. Data from the one Japanese station (KTB) is provided by the Solar Terrestrial Environment Laboratory, Japan, and this station is part of 210 MM chain (http://stdb2.stelab.nagoya-u.ac.jp/mm210/). This work of K.S. is supported by the JSPS Core-to-Core Program, B. Asia-Africa Science Platforms, and JSPS KAKENHI grants 16H06286 and 15H05815. All the other representative magnetic data used in this work are taken from SuperMAG network (http://supermag.jhuapl.edu). The authors are grateful to the PIs of the magnetic observatories and the National institutes that support the observatories based on which the present study is carried out. SuperDARN data are available from the Virginia Tech SuperDARN website (http://vt.superdarn.org/). SuperDARN is a collection of radars funded by national scientific funding agencies of Australia, Canada, China, France, Japan, South Africa, United Kingdom and United States of America. The geosynchronous particle injection data are provided by Los Alamos National Laboratory, USA. The geomagnetic indices and solar wind data are obtained from NASA GSFC CDAWeb (http://cdaweb.gsfc.nasa.gov/). We thank the reviewers for the insightful comments.

References

Abdu, M. A., J. R. Souza, I. S. Batista, B. G. Fejer, and J. H. A. Sobral (2013), Sporadic *E* layer development and disruption at low latitudes by prompt penetration electric fields during magnetic storms, *J. Geophys. Res. Space Physics*, *118*, 2639–2647, doi:10.1002/jgra.50271.

Akasofu, S.-I., and J. K. Chao (1980), Interplanetary shock waves and magnetospheric substorms, *Planet. Space Sci.*, *28*(4), 381–385, doi:10.1016/0032-0633(80)90042-2.

Araki, T. (1977), Global structure of geomagnetic sudden commencements, *Planet. Space Sci.*, *25*(4), 373–384, doi:10.1016/0032-0633(77)90053-8.

Araki, T. (1994), A physical model of the geomagnetic sudden commencement, in *Solar Wind Sources of Magnetospheric Ultra-Low-Frequency Waves*, edited by M. J. Engebretson, K. Takahashi, and M. Scholer, pp. 183–200, AGU, Washington, D. C.

Araki, T., K. Funato, T. Iguchi, and T. Kamei (1993), Direct detection of solar wind dynamic pressure effect on ground geomagnetic field, *Geophys. Res. Lett.*, *20*(9), 775–778, doi:10.1029/93GL00852.

Araki, T., K. Keika, T. Kamei, H. Yang, and S. Alex (2006), Nighttime enhancement of the amplitude of geomagnetic sudden commencements and its dependence on IMF B_z, *Earth Planets Space*, *58*(1), 45–50.

Bittencourt, J. A., and M. A. Abdu (1981), A theoretical comparison between apparent and real vertical ionization drift velocities in the equatorial *F* region, *J. Geophys. Res.*, *86*(A4), 2451–2454, doi:10.1029/JA086iA04p02451.

Chakrabarty, D., R. Sekar, R. Narayanan, C. V. Devasia, and B. M. Pathan (2005), Evidence for the interplanetary electric field effect on the OI 630.0 nm airglow over low latitude, *J. Geophys. Res.*, *110*, A11301, doi:10.1029/2005JA011221.

Chakrabarty, D., R. Sekar, R. Narayanan, A. K. Patra, and C. V. Devasia (2006), Effects of interplanetary electric field on the development of an equatorial spread *F* event, *J. Geophys. Res.*, *111*, A12316, doi:10.1029/2006JA011884.

Chakrabarty, D., D. Rout, R. Sekar, R. Narayanan, G. D. Reeves, T. K. Pant, B. Veenadhari, and K. Shiokawa (2015), Three different types of electric field disturbances affecting equatorial ionosphere during a long duration prompt penetration event, *J. Geophys. Res. Space Physics*, *120*, 4993–5008, doi:10.1002/2014JA020759.

Fejer, B. G., J. W. Jensen, T. Kikuchi, M. A. Abdu, and J. L. Chau (2007), Equatorial ionospheric electric fields during the November 2004 magnetic storm, *J. Geophys. Res.*, *112*, A10304, doi:10.1029/2007JA012376.

Huang, C.-S., K. Yumoto, S. Abe, and G. Sofko (2008), Low-latitude ionospheric electric and magnetic field disturbances in response to solar wind pressure enhancements, *J. Geophys. Res.*, *113*, A08314, doi:10.1029/2007JA012940.

Keller, K. A., M. Hesse, M. Kuznetsova, L. Rastätter, T. Moretto, T. I. Gombosi, and D. L. DeZeeuw (2002), Global MHD modeling of the impact of a solar wind pressure change, *J. Geophys. Res.*, *107*(A7), 1126, doi:10.1029/2001JA000060.

Kelley, M. C., and J. J. Makela (2002), B_y- dependent prompt penetrating electric fields at the magnetic equator, *Geophys. Res. Lett.*, *29*(7), 571–573, doi:10.1029/2001GL014468.

Kikuchi, T., H. Lühr, K. Schlegel, H. Tachihara, M. Shinohara, and T.-I. Kitamura (2000), Penetration of auroral electric fields to the equator during a substorm, *J. Geophys. Res.*, *105*(A10), 23,251–23,261, doi:10.1029/2000JA900016.

Kikuchi, T., K. K. Hashimoto, T.-I. Kitamura, H. Tachihara, and B. Fejer (2003), Equatorial counterelectrojets during substorms, *J. Geophys. Res.*, *108*(A11), 1406, doi:10.1029/2003JA009915.

Kobea, A. T., A. D. Richmond, B. A. Emery, C. Peymirat, H. Lühr, T. Moretto, M. Hairston, and C. Amory-Mazaudier (2000), Electrodynamic coupling of high and low latitudes: Observations on May 27, 1993, *J. Geophys. Res.*, *105*(A10), 22,979–22,989, doi:10.1029/2000JA000058.

Lee, D.-Y., L. R. Lyons, and G. D. Reeves (2005), Comparison of geosynchronous energetic particle flux responses to solar wind dynamic pressure enhancements and substorms, *J. Geophys. Res.*, *110*, A09213, doi:10.1029/2005JA011091.

Lopez, R. E., M. Wiltberger, S. Hernandez, and J. G. Lyon (2004), Solar wind density control of energy transfer to the magnetosphere, *Geophys. Res. Lett.*, *31*, L08804, doi:10.1029/2003GL018780.

Lyatsky, W., G. V. Khazanov, and J. A. Slavin (2010), Alfven wave reflection model of field-aligned currents at mercury, *Icarus*, *209*(1), 40–45, doi:10.1016/j.icarus.2009.11.039.

Lysak, R. L., and D.-h. Lee (1992), Response of the dipole magnetosphere to pressure pulses, *Geophys. Res. Lett.*, *19*(9), 937–940, doi:10.1029/92GL00625.

Namikawa, T., T. Kitamura, T. Okuzawa, and T. Araki (1964), Propagation of weak hydromagnetic discontinuity in the magnetosphere and the sudden commencement of geomagnetic storm, *Rept. Ionosphere Space Res. Jpn.*, *18*, 218–227.

Rastogi, R., and A. Patil (1986), Complex structure of equatorial electrojet current, *Curr. Sci.*, *85*(9), 433–436.

Reinisch, B., and X. Huang (2001), Deducing topside profiles and total electron content from bottomside ionograms, *Adv. Space Res.*, *27*(1), 23–30, doi:10.1016/S0273-1177(00)00136-8.

Sastri, J. H., J. V. S. V. Rao, and K. B. Ramesh (1993), Penetration of polar electric fields to the nightside dip equator at times of geomagnetic sudden commencements, *J. Geophys. Res.*, *98*(A10), 17,517–17,523, doi:10.1029/93JA00418.

Sastri, J. H., Y. Kamide, and K. Yumoto (2003), Signatures for magnetospheric substorms in the geomagnetic field of dayside equatorial region: Origin of the ionospheric component, *J. Geophys. Res.*, *108*(A10), 1375, doi:10.1029/2003JA009962.

Sekar, R., and D. Chakrabarty (2008), Role of overshielding electric field on the development of pre-midnight plume event: Simulation results, *J. Atmos. Sol. Terr. Phys.*, *70*(17), 2212–2221, doi:10.1016/j.jastp.2008.04.015.

Sekar, R., D. Chakrabarty, and D. Pallamraju (2012), Optical signature of shear in the zonal plasma flow along with a tilted structure associated with equatorial spread F during a space weather event, *J. Atmos. Terres Phys.*, *75–76*, 57–63, doi:10.1016/j.jastp.2011.05.009.

Shi, Y., E. Zesta, and L. R. Lyons (2009), Features of energetic particle radial profiles inferred from geosynchronous responses to solar wind dynamic pressure enhancements, *Ann. Geophys.*, *27*(2), 851–859, doi:10.5194/angeo-27-851-2009.

Slinker, S. P., J. A. Fedder, W. J. Hughes, and J. G. Lyon (1999), Response of the ionosphere to a density pulse in the solar wind: Simulation of traveling convection vortices, *Geophys. Res. Lett.*, *26*(23), 3549–3552, doi:10.1029/1999GL010688.

Sofko, G. J., R. Greenwald, and W. Bristow (1995), Direct determination of large-scale magnetospheric field-aligned currents with SuperDARN, *Geophys. Res. Lett.*, *22*(15), 2041–2044, doi:10.1029/95GL01317.

Szuszczewicz, E. P., M. Lester, P. Wilkinson, P. Blanchard, M. Abdu, R. Hanbaba, K. Igarashi, S. Pulinets, and B. M. Reddy (1998), A comparative study of global ionospheric responses to intense magnetic storm conditions, *J. Geophys. Res.*, *103*(A6), 11,665–11,684, doi:10.1029/97JA01660.

Tamao, T. (1964), A hydromagnetic interpretation of geomagnetic SSC*, *Rep. Ionosphere Space Res. Jpn.*, *18*, 16–31.

Tsurutani, B., et al. (2004), Global dayside ionospheric uplift and enhancement associated with interplanetary electric fields, *J. Geophys. Res.*, *109*, A08302, doi:10.1029/2003JA010342.

Wei, Y., W. Wan, B. Zhao, M. Hong, A. Ridley, Z. Ren, M. Fraenz, E. Dubinin, and M. He (2012), Solar wind density controlling penetration electric field at the equatorial ionosphere during a saturation of cross polar cap potential, *J. Geophys. Res.*, *117*, A09308, doi:10.1029/2012JA017597.

Yuan, Z., and X. Deng (2007), Effects of continuous solar wind pressure variations on the long-lasting penetration of the interplanetary electric field during southward interplanetary magnetic field, *Adv. Space Res.*, *39*(8), 1342–1346, doi:10.1016/j.asr.2007.02.033.

Yue, X., W. Wan, J. Lei, and L. Liu (2008), Modeling the relationship between $E \times B$ vertical drift and the time rate of change of h_mF_2 ($\Delta\ h_mF_2/\Delta$ t) over the magnetic equator, *Geophys. Res. Lett.*, *35*(5), L05104, doi:10.1029/2007GL033051.

Zong, Q.-G., B. W. Reinisch, P. Song, Y. Wei, and I. A. Galkin (2010), Dayside ionospheric response to the intense interplanetary shocks-solar wind discontinuities: Observations from the digisonde global ionospheric radio observatory, *J. Geophys. Res.*, *115*, A06304, doi:10.1029/2009JA014796.